Behaviors of Pile Group Installed Near Inclined Ground

경사지반에 인접하여 설치된 무리말뚝의 거동연구

Chae, Kwang-Seok[*1]   채 광 석

Ugai, Keizo[*2]

Yoon, Gil-Lim[*3]   윤 길 림

요 지

사면을 포함한 경사지에 설치된 송전탑, 교각, 고층빌딩 등을 지지하는 말뚝은 풍하중, 지진, 차량 등에 의한 수평하중을 고려하여 설계되어야 한다. 이러한 사면이나 경사지에 설치된 수평하중을 받는 말뚝은 편평한 지반에 비하여, 수평지지력이 감소하기 때문이다. 그러므로 이러한 구조물은 일반적으로 강성이 높고, 대구경의 기초인 피어기초가 사용된다. 수평하중을 받는 피어기초는 일반적으로 장대말뚝과 다른 거동을 한다. 즉, 수평하중에 의하여 말뚝 자체의 회전이 발생하고, 그 회전의 중심점 상부의 사면측의 수동토압에 의존하여 지반파괴가 발생한다는 측면에서 짧은 강성 말뚝과 유사한 거동을 한다. 본 논문은 모래사면의 언덕 근처에 설치된 짧은 말뚝의 수평하중의 영향에 대한 실험 및 수치해석 결과를 포함한다. 대부분을 모형실험과3차원 탄소성 유한요소해석의 비교, 결과를 기술하였다. 먼저, 사면 언덕에서 모형말뚝까지의 거리를 3종류로 구분하여 단항의 모형실험과 군항말뚝의 수평하중 특성을 파악하기 위하여 수평지반과 사면지반(경사30°)에 대하여 말뚝중심간의 거리를 각2종류로 모형실험을 실시하였다. 동시에 3차원 탄소성 유한요소법에 의한 수치해석을 통하여 모형실험의 결과와의 비교를 시도하였다. 사용된 모래지반은 배수조건하에서 삼축압축실험으로 재현하였다. 3차원 탄소성 유한요소해석에서 완전탄소성모델의 파괴기준은 Mohr-Coulomb식, 소성 포텐셜은 Drucker-Prage식을 이용한 MC-DP모델을 적용하였다. 연구결과, 3차원탄소성 유한요소법이 사질토 지반에 설치된 짧은 말뚝의 수평거동을 파악하는데 유효하다는 것을 확인하였다.

Abstract

Many transmission towers, high-rise buildings and bridges are constructed near steep slopes and are supported by large-diameter piles. These structures may be subjected to large lateral loads, such as violent winds and earthquakes. Widely used types of foundations for these structures are pier foundations, which have large-diameters with high stiffness. The behavior of a pier foundation subjected to lateral loads is similar to that of a short rigid pile because both elements seem to fail by rotation developing passive resistance on opposite faces above and below the rotation point, unlike the behavior of a long flexible pile. This paper describes the results of several numerical studies performed with a three-dimensional finite element method (FEM) of model tests of a laterally loaded short pile located near slopes, respectively. In this paper, the results of model tests of single piles and pile groups subjected to lateral loading, in homogeneous sand with 30° slopes and horizontal ground were analyzed by the 3-D FE analyses. The pile was assumed to be linearly elastic. The sand was assumed to have non-associative characteristics, following the MC-DP model. The failure criterion is governed by the Mohr-Coulomb equation and the plastic potential is given by the Drucker-Prager equation. The main purpose of this paper is the validation of the 3-D elasto-plastic FEM by comparisons with the experimental data.

Keywords : 3-D FEM, Group pile, Inclined ground, Lateral load, Rigid pile

*1 Member, Post doc., Korea Ocean Research & Development institute (kschae@kordi.re.kr)
*2 Prof., Dept. of Civil Engrg., Gunma Univ., Japan
*3 Member, Senior Researcher, Korea Ocean Research & Development institute

1. Introduction

Many transmission towers, high-rise buildings and bridges are constructed near steep slopes and are supported by large-diameter piles. These structures may be subjected to large lateral loads, such as violent winds and earthquakes. Widely used types of foundations for these structures are pier foundations, which have large-diameter with high stiffness. Under these loads, the lateral resistances of piles near slopes will be small, compared with piles on horizontal ground. The initial horizontal confining pressure acting on the piles on the slope side is smaller than that in horizontal ground. The behavior of a pier foundation subjected to lateral loads is similar to that of a short rigid pile, because both elements seem to fail by rotation developing passive resistance on opposite faces above and below the rotation point, unlike the behavior of a long flexible pile.

In the past, the design of laterally loaded piles has been based on analytical models in which the soil resistance is obtained empirically, mainly from full-scale tests in the field or model test studies in the laboratory. In soil mechanics and foundation engineering one of the most rigorous numerical modeling methods is the finite element method (FEM). This method can permit realistic three-dimensional effects and computation of soil stresses and deformations around piles. It is also possible to study the progressive development of stresses and deformation in the failure region. The application of the FEM for long flexible piles subjected to lateral loads has been described by several investigators (e.g. [1, 2, 3, 4, 5, 6]). This approach was also used for the numerical studies of the moment carrying capacity of a short pier foundation [7]. Several theoretical methods have been published, which attempted to predict the behavior of field tests and model tests of short rigid piles under lateral loads on horizontal ground [8, 9, 10, 11]. Additional results were published for cases of piles used for slope stabilization purposes and compared with results from the limit equilibrium method [12] and finite element methods [13]. However, there is little published research that attempted to analyze the behavior of a short pile subjected to lateral loads near slopes.

The present research deals with the FE analyses of short rigid piles and located near the crest of a slope, and their comparison with the measurements of model tests. The results of model tests of single piles and pile groups subjected to lateral loading in homogeneous sand with 30° slopes are analyzed by the 3-D elasto-plastic FEM. To compare with slope cases, cases of piles located in horizontal ground are also investigated. Series of single short pile tests were conducted to investigate the effect of horizontal distance from the pile to the crest of the slope. In short pile groups, focus was placed on the pile group efficiency and the behavior of each pile, considering the influences of the pile spacing and the pile cap. The model pile had a constant embedment depth / diameter (D_E / D) ratio of 5.0 in all tests.

2. Model Tests and Finite Element Analyses

2.1 Model Tests and Procedure

Model tests were conducted in dry sand and its physical properties are listed in Table 1. The triaxial compression test of soil in a dense state, with a relative density Dr of 90%, gave a peak friction angle ϕ of 47.5°. Using a hopper with a 2 mm sieve, the sand was poured to make up a homogeneous horizontal ground. The 30o slope surface was formed by excavation. The model pile was made of smooth aluminum with a wall thickness of 3 mm and outside diameter of 100 mm. It was buried 500 mm deep in the ground for a constant embedment depth / diameter (D_E / D) ratio of 5.0 in all the tests.

The pile was instrumented with 10-coupled strain gauges placed on the two opposite faces in the lateral loading direction. Lateral loads were applied to the pile

Table 1. Physical properties of the sand

Specific gravity	G_s	2.723
Average grain size	D_{50} (mm)	0.201
Uniformity coefficient	U_c	2.122
Coefficient of curvature	$U_c{}'$	0.912
Maximum void ratio	e_{max}	0.951
Minimum void ratio	e_{min}	0.599

head by a motor, which was 100 mm above the ground surface. The loads were measured through a load cell, and the pile head displacements were recorded with a displacement transducer at the point of load application.

There are several interrelated factors that affect the lateral resistance of a pile and the dominant one is the pile stiffness, which determines whether the pile behaves rigidly, causing a rotation. One simple criterion for rigidity is the pile depth (D_E) in relation to its diameter (D), related to the stiffness ratio (E_e/G^*) [1]. Short piles can be described as having intermediate stiffness whenever the (D_E / D) ratio is bounded [15], as follows;

$$0.05\left(\frac{E_e}{G^*}\right)^{1/2} < \frac{D_E}{D} < \left(\frac{E_e}{G^*}\right)^{2/7}$$ (1)

$$G^* = \left(\frac{E_s}{2(1+\nu)}\right)\left(1 + \frac{3\nu}{4}\right)$$ (2)

where, the equivalent shear modulus of the soil G^*, the effective Young's modulus of the pile E_e ($= (EI)_p/(\pi B^4/64)$).

For a homogeneous soil used in this model test, G^* is related to the horizontal Young's modulus of the soil E_s (25.8 MPa) and Poisson's ratio ν (0.3). For a rigid pile, calculated bounds of (D_E / D) ratio are 7.5 - 1.75, indicating that this pile ((D_E / D) ratio = 5.0) can be considered as a short rigid pile. The pile rigidity is also related to a stiffness factor T [16]. In cohesionless soils, T is calculated as,

$$T = \sqrt[5]{\frac{E_p I_p}{n_h}}$$ (3)

where $E_p I_p$ is the bending stiffness of the pile and n_h is the coefficient of subgrade reaction.

The embedment depth of the pile has to be less than 2T to be considered as a short rigid pile and greater than 4T for behavior as a long elastic pile [9, 17]. For the model pile, the depth of embedment was 500 mm, giving a (D_E / D) ratio of 5.0 while the value of 2T was estimated as 656 - 800 mm (possible range of values for n_h= 7.5 - 20 MN/m^3 for medium-dense to dense sands [18]). Furthermore, the value of nh decreases near the crest of the slope, the computed value of 2T can therefore

be considered to be large enough to satisfy the criterion for a short rigid pile.

2.2 Three-dimensional Elasto-plastic Modeling

The constitutive law defines the relationship between strain and stress, and in the elastic region this relationship is linear in most cases, represented by Young's modulus E and Poisson's ratio ν. However, only few materials might be described by the elastic behavior and the elasto-plastic behavior applies to most commonly used materials. Thus the elasto-plastic model would be more appropriate for the numerical analyses. The plastic region starts with the yielding point and is then described in terms of work hardening. Clearly, difficulties arise with specifying the yielding point and the description of the plastic region, which vary from material to material. In the terminology of plasticity the ideal material used to represent the soil was assumed to follow the elasto-perfectly plastic model.

The pile was assumed to be linearly elastic. The sand was assumed to have non-associative characteristics, following the MC-DP model. The failure criterion is governed by the Mohr-Coulomb equation and the plastic potential is given by the Drucker-Prager equation. Such a combination is useful for the improvement of the convergence of the FE calculations [14].

Taking differences in the initial stress conditions of the ground (e.g. slope, horizontal ground) into consideration, calculations in the FE analysis were carried out in a two-step process. In the first step, the initial stress condition due to the dead weight of the soil was calculated using the shear strength reduction finite element method (SSR-FEM) [19], without taking the existence of the pile into consideration. The second step was to simulate the behavior of the soil as the lateral displacement at the pile head is applied incrementally. The iterative elasto-plastic computations were carried out using the modified Newton-Raphson method.

The material parameters used in the analyses are summarized in Table 2. The friction angle ϕ of the sand was 47.5° with a relative density Dr of 90% based on

Table 2. Model parameters used in the FE analyses

	Pile Pile cap	Sand	Frictional element (soil—pile interface)
Young's modulus E (kPa)	6.86E+07	Eq. (4)	Eq. (4)
Poisson's ratio ν	0.345	0.3	0.3
Unit weight γ (kN/m³)	26.4	15.68	15.68
Friction angle ϕ (Degree)	−	47.5	25
Dilatancy angle Ψ (Degree)	−	17.5	0

$$E_{50} = E_0 \, (\sigma_m / \sigma_0)^n$$

$$E_0 = 1143 \text{ kPa}, \quad \sigma_0 = 1 \text{ kPa}, \quad n = 0.8311, \quad \sigma_m = \sigma(\sigma_1 + \sigma_2 + \sigma_3) / 3 \qquad (4)$$
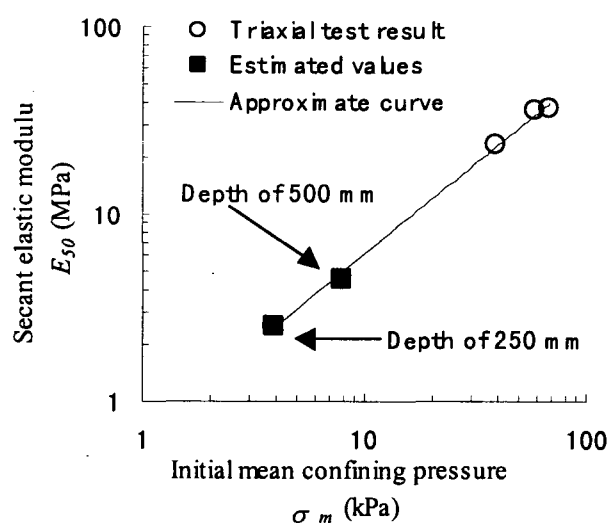
Fig. 1. Exponential-fitting curve based on the result of the triaxial test

the triaxial test results. The dilatancy angle Ψ of the sand was evaluated according to the equation [20]: $\Psi = \phi - 30°$ Values of Poisson's ratio ν generally lay between 0.25 and 0.35 in the sand, and therefore 0.3 was used. It should be noted that we used the secant elastic modulus E_{50} measured in the tests in Eq. (4). As shown in Figure 1, the relationship between the secant elastic modulus E_{50} and the initial mean confining pressure σ_m on log-log axes is assumed linear. The approximate line, from which the values of E_{50} were obtained from the drained triaxial compression test, allows estimating the values at different ground depths in the analysis. Each estimated E_{50} at the depth of 250 and 500 mm is also indicated in this figure. Thin frictional brick elements were inserted between the pile and the sand in order to consider the slippage at the pile-soil interface. The friction angle ϕ of the frictional element was determined to be 25°, based on the results of slippage tests between an aluminum plate and the sand. The dilatancy angle Ψ of the frictional elements was assumed to be zero and other material constants of these elements were the same as the surrounding sand.

2.3 Single Short Pile Near Slope in Model Test and 3-D FE Analysis

Several cases of model tests for single short piles are shown in Table 3. The single short pile model tests were conducted considering 3 different horizontal distances beyond the crest of the slope (0D, 2D, 4D (D: diameter of pile)). To compare with the slope effect, analysis of the horizontal ground case was also performed.

Figure 2 is a sketch of the model test apparatus and a typical 3-D FE mesh for a short single pile consisting of 20 node brick elements. As shown in Figure 2 (b),

Table 3. Model test conditions of single pile

Test pattern	Ground shape	Distance from the crest of slope (D = Diameter of pile)
S-H	Horizontal ground	−
S-0D		0D
S-2D	Slope (30°)	2D (=200 (mm))
S-4D		4D (=400(mm))
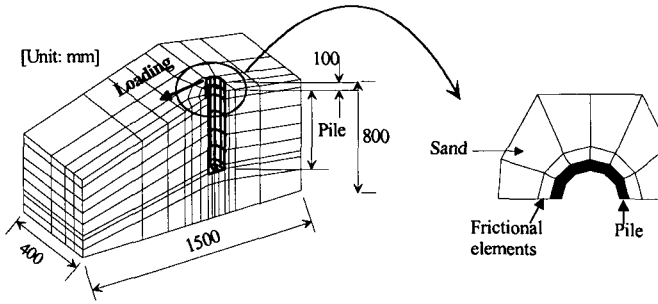
(a) Sketch of single pile test apparatus
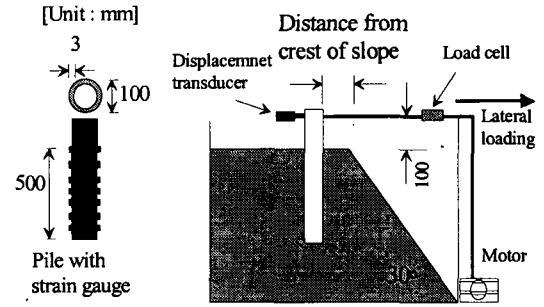
(b) 3-D FE meshes in the single pile

Fig. 2. Lateral loading model test of short single pile and 3D-FE mesh (slope case)

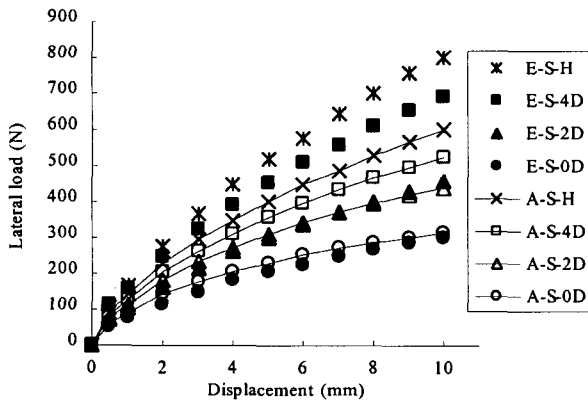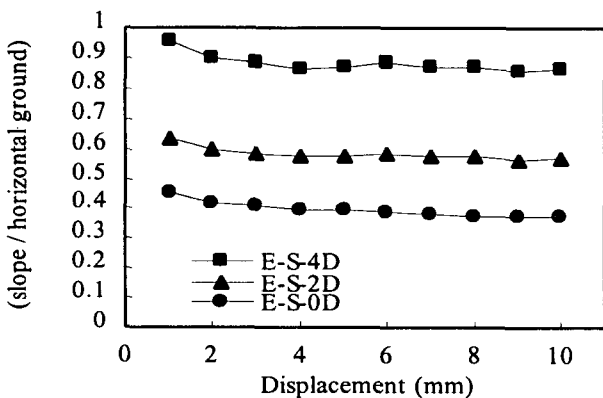E – Experimental result
A – Analytical result

Fig. 3. Loading vs. displacement curves in single pile tests

half the domain was eliminated by taking advantage of the symmetry with respect to the center plane parallel to the loading direction. The plane of symmetry was a

smooth boundary. Other side boundaries and the bottom boundary were fixed. Thin frictional brick elements were inserted between the pile and the soil in order to consider the potential for slippage at the pile-soil interface.

Figure 3 shows the experimental and analytical lateral load-displacement curves for short single piles. These displacements were measured at the point of load application. There is no observed peak strength in the experimental and analytical results shown in this figure. The experimental results for cases "E-S-H" and "E-S-4D" are underestimated by the analyses. Nevertheless, the data show reasonable agreement between the experimental and analytical curves for the piles near a slope. It is found, due to the slope effect, that the lateral resistance of the pile decreases, as the location of the pile is closer to the crest of the slope.

Figure 4 shows the relationship between the load ratio and displacement at the loading point. It should be noted

(a) Experimental result
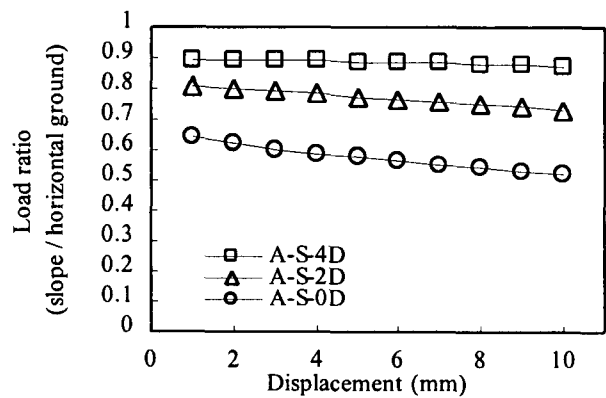
(b) Analytical result

Fig. 4. Normalized loading vs. displacement curves in single pile tests

that for each case (0D, 2D, 4D) the load for a pile in the slope is normalized by the load in the horizontal ground case at the same displacement. It is found that the value of load ratio is affected markedly in the small displacement range by the distance of the pile to the crest of the slope. However, the load ratio has a constant value as the displacement increases.

The value of load ratio is approximately 0.9 when the pile is located at a distance equal to 4D from the crest of the slope in both the experimental and analytical results. Even in this case, the difference between the horizontal ground and the slope condition is clear. To obtain a load ratio = 1.0 (equivalent to the horizontal ground condition), it may be necessary to move the pile to a distance larger than 4D from the crest of the slope. The strain gauges fixed on the piles give the bending strains during lateral loading. Initially, the preliminary fitting of each bending strain is calculated by cubic spline functions. On the fitted bending strains, the bending moment profile is approximated by a fifth order polynomial with the bending stiffness EI and the pile radius r. The pile head is free to rotate; therefore, bending moment values should be zero at the pile head. The subgrade reaction profile, p(z) is evaluated by differentiating the bending moment profile M(z) twice with respect to the depth z, by making use of the beam theory, according to Eq. (5):

$$p(z) = \frac{1}{D} \frac{\partial^2 M(z)}{\partial z^2}$$

(5)

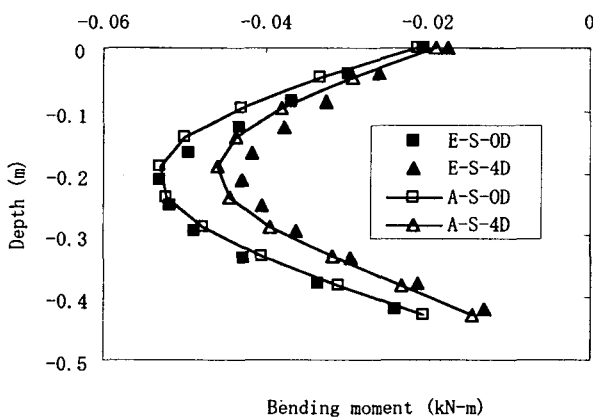where D is the pile diameter.

The recorded bending moment curves, which show the distribution of the bending moment at the lateral load of 196 N, are shown in Figure 5. The analytical data show reasonable agreement with the experimental results. The maximum moments occur at about 40% of the embedded depth of the pile. The value of moment increases regularly as the location of the pile approaches the crest of the slope at the same load applied.

Figure 6 shows the subgrade reaction distributions at the lateral load of 196 N in the experimental and analytical results, respectively. The depth of the zero subgrade reaction point is shifted slightly downward as the distance of the pile to the crest of the slope gets closer. This may be caused by a release of the confining pressure around the pile closer to the crest.

Figure 7 shows the calculated failure regions when the pile head reaches the lateral load of 196 N. The failure region, which indicates whether any Gauss points fail or not, is determined from the concept of local safety factor (LSF). LSF is derived from the Mohr-Coulomb equation. The case when the value of LSF is equal to 1.00 is considered as the failure of the soil element, shown in black in the figure. From these comparisons, it is found that the failure region gets wider, as the distance of the pile to the crest becomes closer.
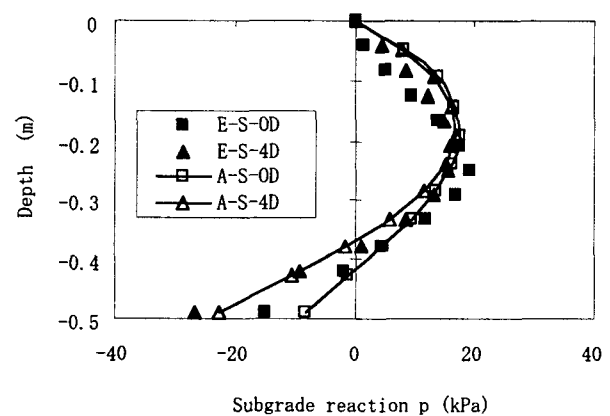

Fig. 5. Distributions of bending moment at loading of 196 N from single pile tests

Fig. 6. Subgrade reaction curves at loading of 196 N from single pile tests

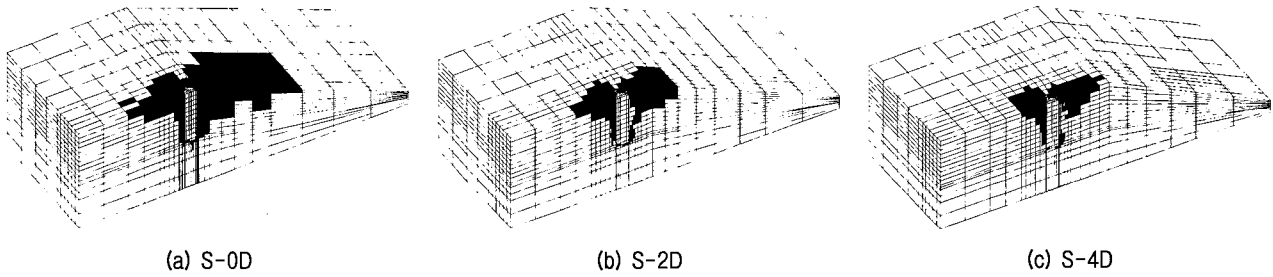(a) S-0D   (b) S-2D   (c) S-4D

Fig. 7. Calculated failure regions at the load 196 N

2.4 Short Pile Groups Near Slope in Model Test and 3-D FE Analysis

This study is an extension of the work, which describes the model test and the FE analysis of laterally loaded short single piles located near slopes. Intuitively, short pile groups located near slopes should have a significant effect upon the pile response to lateral loading, however, relatively little information is available to guide designers in quantifying this effect.

Model pile tests were carried out to investigate the behavior of the laterally loaded short pile groups located at the crest of 30° slopes. To assess the slope effect in short pile groups, the model tests and analyses for horizontal ground cases were also performed. It should be necessary to investigate the influence of interaction factors such as the pile spacing and the fixed condition of the pile head, for short pile groups subjected to lateral
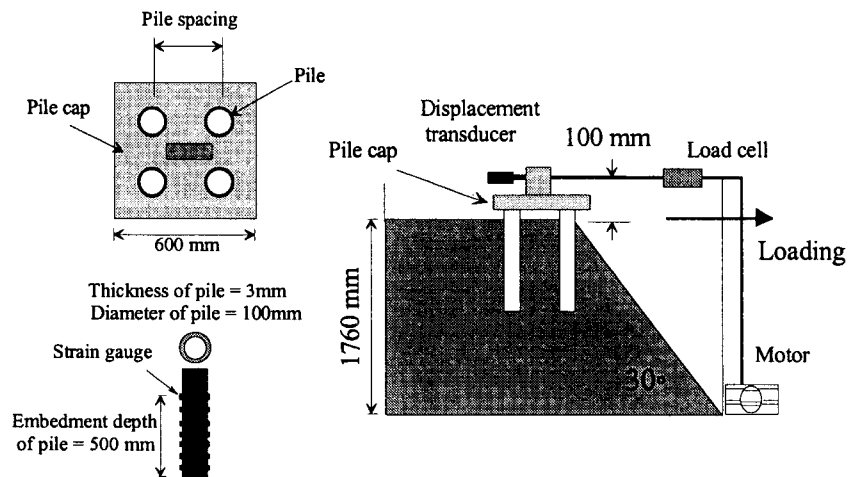
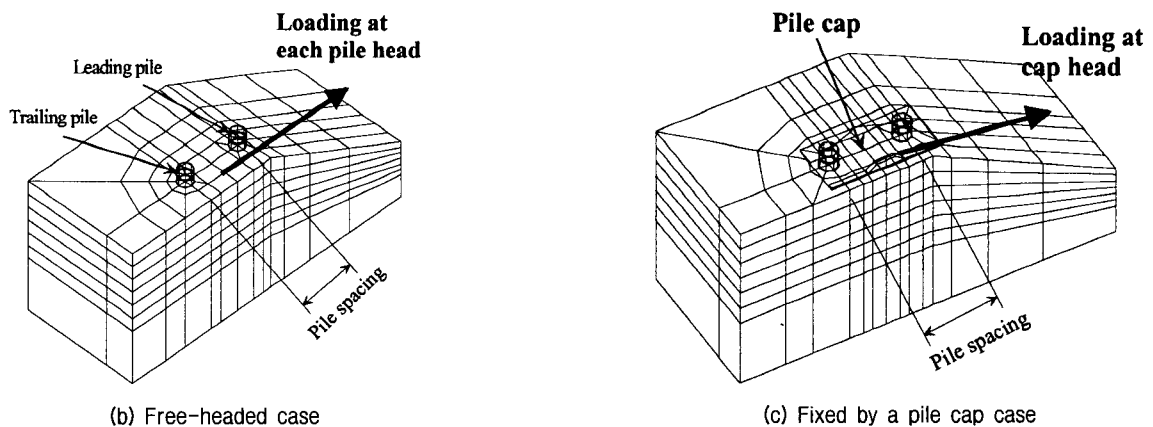(a) Sketch of the pile group test apparatus

(b) Free-headed case   (c) Fixed by a pile cap case

Fig. 8. Lateral loading model tests of a short pile group and 3D FE mesh (slope case)

Table 4(a). Experimental model tests

Test pattern	Ground shape	Pile spacing (D = Diameter of pile)	Fixed condition
E-H-2D	Horizontal ground	2D (= 200 (mm))	Fixed by a pile cap
E-H-4D		4D (= 400 (mm))	
E-S-2D	Slope (30°)	2D	
E-S-4D		4D	

Table 4(b). FEM Analyses

Test pattern	Ground shape	Pile spacing (mm) (D = pile diameter)	Fixed condition
A-H-2D	Horizontal ground	2D (= 200 (mm))	Fixed by a pile cap
A-H-4D		4D (= 400 (mm))	
A-S-2D	Slope (30°)	2D	
A-S-4D		4D	
A-H-2D-F	Horizontal ground	2D	
A-H-4D-F		4D	
A-S-2D-F	Slope (30°)	2D	Free-headed
A-S-4D-F		4D	

loading.

Figure 8 shows a short pile group consisting of four piles, arranged in a 2-by-2 square, on a 30° slope. For the group pile in the model test and analysis, the material parameters of the sand and the piles were the same as those of the single pile test. The pile cap, a plate with a dead load of 0.2 kN, was not in contact with the ground surface. The piles positioned in the front row and back row from the loading direction will be referred to as leading piles and trailing piles, respectively. The leading piles were adjacent to the crest of the slope. In the same way as single model tests, lateral loads were applied to the pile cap and the displacements were measured at the point of load application.

The 3-D FE meshes, used for two different kinds of pile cap conditions calculated in the analyses are shown in Figures 8 (b) and (c). Half of the domain was eliminated because of the symmetry defined by the center plane parallel to the loading direction. Figure 8 (b) shows the free-headed case, which is to investigate only the interaction of pile-soil-pile by two different patterns of pile spacing (2D, 4D (D: pile diameter)). Therefore, each pile head was loaded directly, so it could rotate freely like a single pile. Figure 8 (c) shows the case fixed by

a pile cap for taking the influences of both the fixed condition and the pile spacing into consideration, which was the same fixed condition as the experimental model tests. The details of each series of experimental model tests and analyses are summarized in Table 4. Pile spacing indicates the distance between the pile centers.

Figure 9 shows the experimental and analytical relationships between the lateral load and the displacement at the loading point in short pile groups. It is clear that the lateral resistance of pile groups located near a slope is smaller than that found for the same groups in
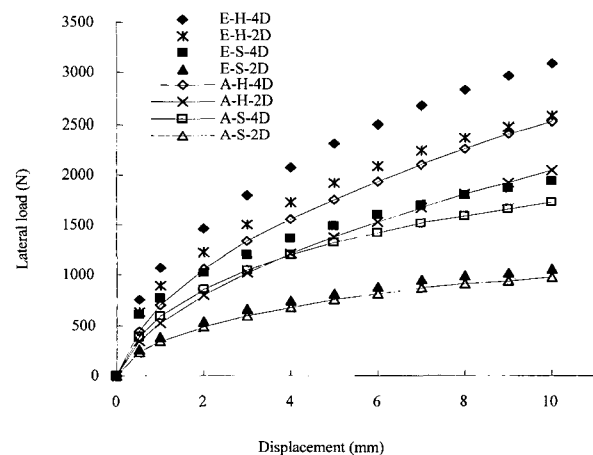

Fig. 9. Loading vs. displacement curves for each pile group case

horizontal ground. A reduction in pile spacing decreases the resistance of the pile group in both the horizontal ground and the slope.

The efficiency of the pile group (e) is a convenient way to modify the single pile response to account for group effects. Efficiency is defined at a given displacement as,

$$e = \frac{Load_{(pile\ group)}}{n \times Load_{(single)}} \quad (n = the\ number\ of\ piles\ within\ the\ group) \quad (6)$$

Figure 10 shows the relationship between the pile group efficiency and the lateral displacement for the horizontal ground and the slope, respectively. It can be found that the analytical results for the cases fixed by

a pile cap agree with the experimental results better than for the free-headed cases. It is clear that the group efficiency is higher as the pile spacing is larger. The efficiency for the case fixed by a pile cap is much greater than that for the free-headed case according to the analysis. From Figure 10(a), it can be seen that the group efficiency of each pile group on the horizontal ground is almost constant irrespective of the displacements. However, the group efficiency in case of the slope is high for small displacements and decreases as the displacement increases, as shown in Figure 10(b).

The analytical load distribution ratio for the leading piles as a function of the lateral displacement is presented in Figure 11. The load distribution ratio of each pile
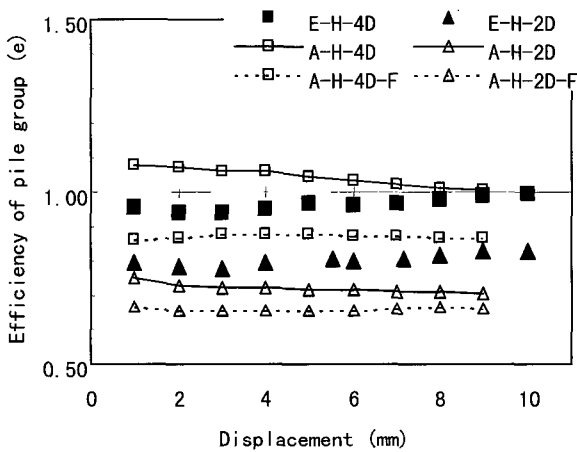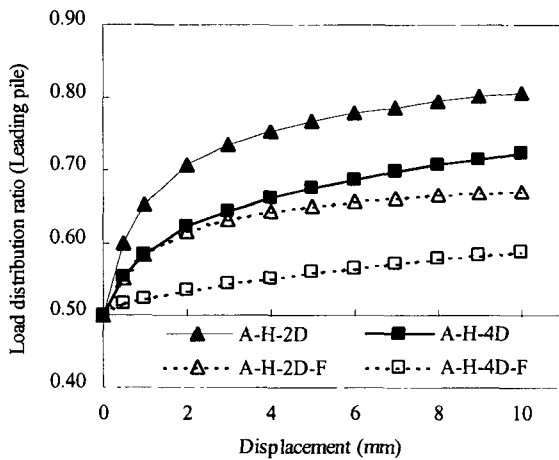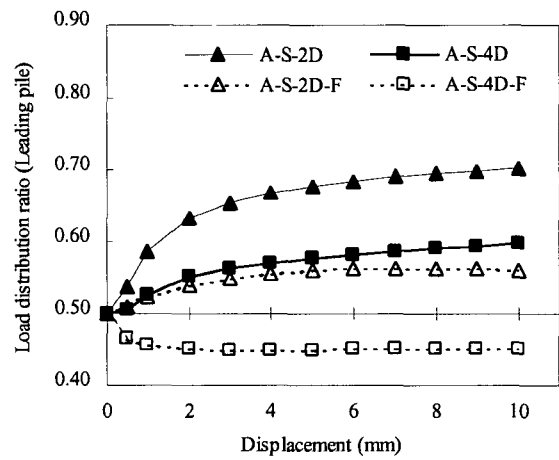

(a) Horizontal ground
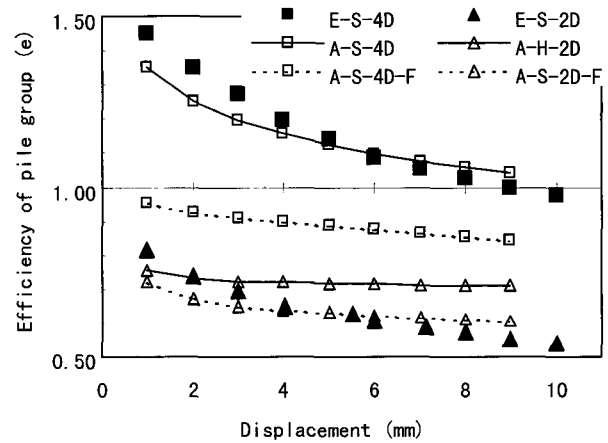
(b) Inclined ground (slope)

Fig. 10. Pile group efficiency for each pile group


(a) Horizontal ground

(b) Inclined ground (slope)

Fig. 11. Load distribution ratio for leading piles from two different grounds

within the pile group is determined from the shear force calculated at each pile head. The load distribution ratios of the leading piles decrease as the pile spacing gets larger. This response is related to the effect of the leading piles on the yield zones developed in the soil ahead of the trailing piles. The reduction of the ratio for leading piles is more significant for the free-headed cases than for the fixed-headed cases. The leading piles are subjected to a much larger load than trailing piles in the horizontal ground, as shown in Figure 11 (a). It should be noted that both leading and trailing piles have initially the same horizontal resistance. However, the pile groups located near the slopes have initially different horizontal resistance between the leading and trailing piles, because of the

reduced initial confining pressure for leading piles near the crest of the slope. As shown in Figure 11 (b), the case of "A-S-4D-F", which corresponds to free-headed piles in a slope with pile spacing of 4D, shows the load distribution ratio of the leading piles less 0.5 than. It should be noted that the load distribution ratio of the leading piles gets smaller with increasing pile spacing in the free-headed piles.

Figures 12 and 13 show the displacement distributions along the piles as a function of depth for the free-headed case and the cases of piles fixed by a pile cap in slopes; data are plotted for the leading piles in the pile groups at pile spacing of 2D and 4D. The curve labeled "single pile-0D" represents a single pile test at the same location
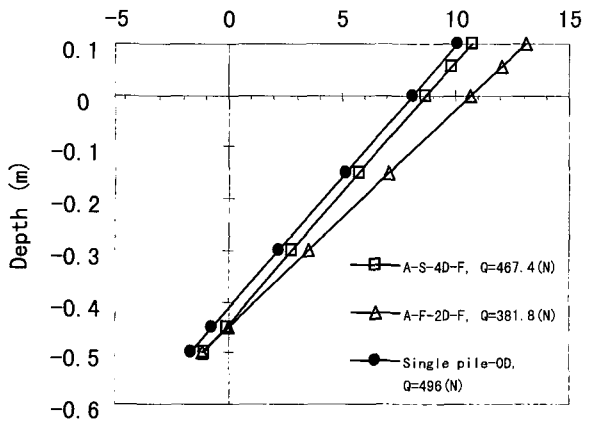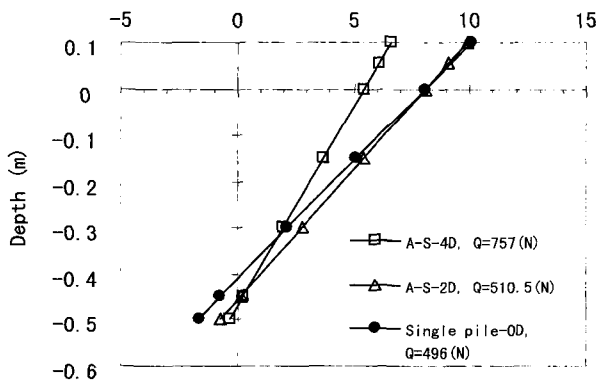

Horizontal displacement/Pile head load (mm/kN)

(a) Horizontal displacement
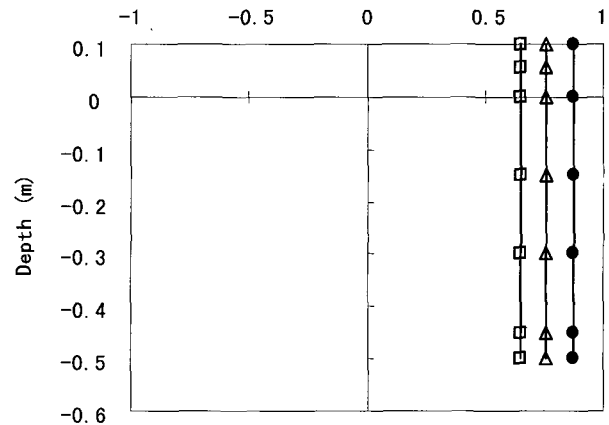
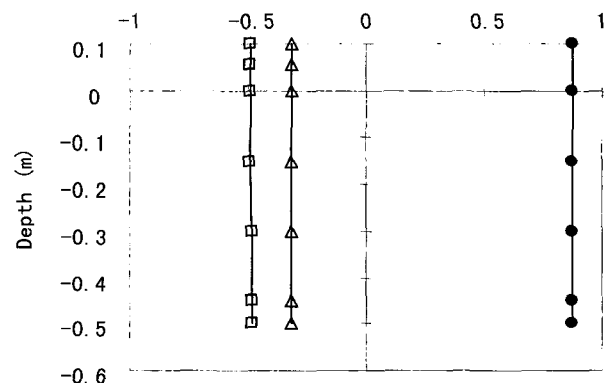Vertical displacement/Pile head load (mm/kN)

(b) Vertical displacement

Fig. 12. Displacement distributions for leading piles (free-headed case in slope)

Horizontal displacement/Pile head load (mm/kN)

(a) Horizontal displacement

Vertical displacement/Pile head load (mm/kN)

(b) Vertical displacement

Fig. 13. Displacement distributions for leading piles (fixed by a pile cap case in slope)

as the leading pile in the pile groups. These plots are shown for the load that produces 5mm of lateral displacement at the pile head. The shear force (Q) at the pile head in each case is different, as indicated in the figures. The displacement values were normalized by the shear force at the pile head in order to facilitate the comparison. As presented in Figure 12(a) and Figure 13(a), the normalized horizontal displacements of the leading piles get smaller as the pile spacing gets wider.

The rotation point (zero horizontal displacement point) of the pile groups occurs at a slightly greater depth than that of the single pile, with no variation of its depth irrespective of the pile spacing. In the normalized vertical displacements (Fig. 12(b) and Fig. 13(b)), the vertical displacements of the leading piles move in different directions. Plus sign indicates that a pile moves in the upward direction. Leading piles of the free-headed cases are uplifted like a single pile. However, leading piles fixed by a pile cap are pushed downward. Trailing piles of both cases move in the upward direction.

3. Conclusions

The main purpose of this paper is to find out that the 3-D elasto-plastic FEM is very effective in evaluating the lateral resistance of a short pile placed on near slopes. Based on model tests and numerical modeling, several conclusions can be issued as follows:

1) The behaviors of model piles were analyzed by the three-dimensional finite element analyses. The sand was assumed to be an elasto-perfectly plastic material with non-associative characteristics, following the MC - DP model. Parameter values for the sand were determined from triaxial compression tests.

2) The lateral resistance of the single short pile decreases, as its location is closer to the crest of the slope. The reduction of the lateral resistance due to the slope effect is influenced markedly in the small displacement range and is not so changed as the displacement increases.

3) For a short pile group near the crest of a slope, a significant reduction in the group efficiency is observed

as the displacement of pile head increases. Nevertheless, the group efficiency on the horizontal ground appears to be relatively constant.

4) The load distribution ratio of the leading piles decreases as the pile spacing gets larger. This response is related to the effect of the leading piles on the yield zones developed in the soil ahead of the trailing pile. The reduction of the ratio for the leading piles is more significant for the free-headed cases than for the cases of piles fixed by a pile cap.

5) In short pile groups located near the crest of the slope, the rotation point of the leading piles occurs at a slightly greater depth than that of the single pile, with no variation of its depth irrespective of the pile spacing.

References

1. Randolph, M. F. (1981), "The response of flexible piles to lateral loading", *Geotechnique*, Vol.31, pp.247-259.

2. Kimura, M., Adachi, T., Kamei, H., and Zhang, F. (1995), "3-D finite element analyses of the ultimate behavior of laterally loaded cast-in-place concrete piles", *Proc. of the 15th Int. Symp. On Numerical Models in Geomechanics*, Davos, Switzerland, pp.589-594.

3. Chatani, F. and Nishiyama, T. (1995), "Behaviour of lateral loaded pile near a cliff", *J. Struct. Constr. Eng.* AIJ (in Japanese), Vol.478, pp.115-124.

4. Brown, D.A. and Shiethree, C.F. (1990), "3-dimensional finite element model of laterally loaded piles", *Computers and Geotechnics*, Vol.10(1), pp.59-79.

5. Desai, C. S. and Kuppusamy, T. (1980), "Application of a numerical procedure for laterally loaded structures", *Numerical Methods in Offshore Piling*, ICE, pp.93-99.

6. Wakai, A., Gose, S., and Ugai, K. (1999), "3-D elasto-plastic finite element analyses of pile foundations subjected to lateral loading", *Soils and Foundations*, Vol.32, pp.97-111.

7. Laman, M., King, G.J.W., and Dikin, E.A. (1999), "Three-dimensional finite element studies of the moment-carrying capacity of short pier foundations in cohesionless soil", *Computer and Geotechnics*, Vol.25, pp.141-155.

8. Brinch Hansen, J. (1961), *The ultimate resistance of rigid piles against transversal forces*, Danish Geotechnical Institute, Copenhagen, Bulletin Vol.12, pp.5-9.

9. Broms, B. B. (1964), "Lateral resistance of piles of cohesionless soils", ASCE *J. of SMFE Div.*, Vol.90, pp.123-156.

10. Petrasovits, G. and Award, A. (1972), "Ultimate lateral resistance of a rigid pile in cohesionless soil", *Proc., 5th European Conf. on SMFE*, Madrid, Vol.3, pp.407-412.

11. Meyerhof, G.G. Mathur, S. K., and Valsangkar, A. J. (1981), "Lateral resistance and deflection of rigid wall and piles in layered soils", *Can. Geotech. J.*, Vol.18, pp.150-170.

12. Ito, T. and Matsui, T. (1975), "Methods to estimate lateral force acting on stabilizing piles", Soils and Foundations, Vol.15(4), pp.43-59.

13. Cai, F. and Ugai, K. (2000), "Numerical analysis of the stability of a slope reinforced with piles", Soils and Foundations, Vol.40(1), pp.73-84.

14. Tanaka, T. (1992), Deformation and stability analysis by finite element method, in Principle of Soil mechanics (first revision), The Japanese Geotechnical Society (in Japanese).

15. Carter, J. P. and Kulhawy, F.H. (1992), "Analysis of laterally loaded shafts in rock", ASCE J. of Geotech. Eng., Vol.118(6), pp.839-855.

16. Matlock, H. and Reese, L. C. (1960), "Generalized solutions for laterally loaded piles", ASCE J. of SMFE Div.; Vol.86(5), pp.63-91.

17. Chari, T. R. and Meyerhof, G. G. (1983), Ultimate capacity of rigid single piles under inclined loads in sand, Can. Geotech. J., Vol.20, pp.849-854.

18. Terzaghi, K. (1955), Evaluation of coefficients of subgrade reaction, Geotechnique, Vol.5, pp.297-326.

19. Ugai, K. and Leshchinsky, D. (1995), Three-dimensional limit equilibrium and finite element: a comparison of results, Soils and Foundations, Vol.35(4), pp.1-7.

20. Tatsuoka, F. (1993), Relationships between the stress and strain increments, in Introduction to strength of soils and failure of ground (third revision), The Japanese Geotechnical Society (in Japanese).